IEEE Access
Multidisciplinary | Rapid Review | Open Access Journal

SPECIAL SECTION ON ARTIFICIAL INTELLIGENCE FOR PHYSICAL-LAYER WIRELESS COMMUNICATIONS

Received February 20, 2020, accepted March 5, 2020, date of publication March 12, 2020, date of current version March 24, 2020.

Digital Object Identifier 10.1109/ACCESS.2020.2980285

Deep Learning-Based mmWave Beam Selection for 5G NR/6G With Sub-6 GHz Channel Information: Algorithms and Prototype Validation

MIN SOO SIM[1], (Student Member, IEEE), YEON-GEUN LIM[2], (Member, IEEE), SANG HYUN PARK[1], (Student Member, IEEE), LINGLONG DAI[3], (Senior Member, IEEE), AND CHAN-BYOUNG CHAE[1], (Senior Member, IEEE)

[1]School of Integrated Technology, Yonsei University, Seoul 03722, South Korea
[2]Samsung Electronics, Seoul 06765, South Korea
[3]Department of Electronic Engineering, Tsinghua University, Beijing 100084, China

Corresponding author: Chan-Byoung Chae (cbchae@yonsei.ac.kr)

This work was supported in part by the Institute of Information and Communications Technology Planning and Evaluation (IITP) funded by the Korea Government (MSIT) under Grant 2019-0-00685 and Grant 2018-0-00170, and in part by the National Natural Science Foundation of China for Outstanding Young Scholars under Grant 61722109.

ABSTRACT In fifth-generation (5G) communications, millimeter wave (mmWave) is one of the key technologies to increase the data rate. To overcome this technology's poor propagation characteristics, it is necessary to employ a number of antennas and form narrow beams. It becomes crucial then, especially for initial access, to attain fine beam alignment between a next generation NodeB (gNB) and a user equipment (UE). The current 5G New Radio (NR) standard, however, adopts an exhaustive search-based beam sweeping, which causes time overhead of a half frame for initial beam establishment. In this paper, we propose a deep learning-based beam selection, which is compatible with the 5G NR standard. To select a mmWave beam, we exploit sub-6 GHz channel information. We introduce a deep neural network (DNN) structure and explain how we estimate a power delay profile (PDP) of a sub-6 GHz channel, which is used as an input of the DNN. We then validate its performance with real environment-based 3D ray-tracing simulations and over-the-air experiments with a mmWave prototype. Evaluation results confirm that, with support from the sub-6 GHz connection, the proposed beam selection reduces the beam sweeping overhead by up to 79.3 %.

INDEX TERMS 5G NR, 6G, mmWave, beamforming, deep learning, beam selection, and ultra-low latency.

I. INTRODUCTION

After Long Term Evolution (LTE), fifth-generation (5G) cellular network technology has emerged to fulfill requirements to support various services including enhanced mobile broadband (eMBB), ultra-reliable and low-latency communication (URLLC), and massive machine-type communications (mMTC) [1]. Among these services, the one to have attracted the most attention is the first mentioned—eMBB. The main aim of eMBB, which is a progression from the fourth generation (4G) LTE mobile broadband service, is to provide a very high data rate. To achieve this requirement, various technologies have been studied and developed, and the 5G network has been globally standardized by the 3rd Generation Partnership Project (3GPP) as 5G New Radio (NR).

In eMBB service, researchers' efforts have mainly followed two paths—increasing spectral efficiency (bps/Hz) and widening frequency bandwidth (Hz). In the latter case, as spectrum resource is quite limited in the sub-6 GHz band, researchers have been tried to exploit wider bandwidth in the millimeter wave (mmWave) band (above 10 GHz) [2], [3]. However, the mmWave band faces, by nature, several obstacles such as high pathloss, blockage, and high oxygen absorption. Therefore, to implement mmWave cellular

The associate editor coordinating the review of this manuscript and approving it for publication was Guan Gui.

networks, base stations, next generation NodeBs (gNBs) in NR, are densely deployed, and directional antennas are employed. Also, researchers have considered implementing an antenna array consisting of a number of small-size antennas, thanks to a short wavelength. With multiple antennas, a signal can form a narrow beam with a high gain by adjusting phase or amplitude of each antenna. This technique, so-called beamforming, causes a highly directional link between a gNB and a user equipment (UE). As the beam has a very narrow beamwidth, there should be fine beam alignment between the gNB and the UE, which is known as beam management [4], [5].

The goal of beam management is selecting and retaining a proper beam pair, a transmitter-side beam and a corresponding receiver-side beam, that can provide good connectivity. Generally, beam management can be categorized as initial beam establishment for idle UEs and beam tracking for connected UEs. The former establishes a connection between a gNB and a UE, while the latter compensates movements of UEs and environments. Due to its importance in enabling mmWave communications, various approaches for initial beam establishment have been studied [6]–[11]. In this paper, we focus on the initial beam establishment (or beam selection). In 5G NR, a major part of beam selection procedures is taken up with by *beam sweeping*. This procedure exhaustively searches for the beam providing the strongest signal strength. As it must search in all possible directions for the best performance, beam selection takes a long time, which is critical to user experience in 5G NR and the sixth-generation (6G) communications.

Recently, the concept of deep learning has been widely studied and applied to various fields such as image recognition and natural language processing [12]. Deep learning, by nature, is a useful technique that optimizes a deep neural network (DNN) that can approximate mapping of unknown or nonlinear relationships. Therefore, it has been adopted in the field of wireless communications for modulation [13], detection [14], [15], channel estimation [16], non-orthogonal multiple access (NOMA), massive multiple-input multiple-output (MIMO) systems [17], etc. Researchers also have applied deep learning to resolve the beam management problem [18]–[27]. Some of prior works need additional information such as position [18]–[20] or LIDAR [21]. For initial beam establishment, however, it may not be feasible in the 5G NR standard to rely on additional components such as the global positioning system (GPS) or LIDAR. In [22], a deep learning-based coordinated beamforming was proposed, where the input of the DNN is the received orthogonal frequency-division multiplexing (OFDM) symbols from multiple gNBs. The deep learning-based beamforming strategy that, in single-scattering-path environments, employs angles of arrival as the input of the DNN was proposed in [23]. As the input data, the former exploits the received signal directly, while the latter estimates channel characteristics. However, both methods have a limitation that a mmWave link has to be established before it gathers the input data, which does not fit with initial beam establishment.

In this paper, we propose a deep learning-based beam selection that, unlike prior works, exploits channel state information (CSI) of a sub-6 GHz channel to choose a mmWave beam. Due to its wide cell size, it is reasonable to assume the sub-6 GHz link is established [28], [29]. Assuming sub-6 GHz access is established in advance, we can utilize CSI without concern for time- and frequency-domain synchronization. Taking advantage of the sub-6 GHz information, one can reduce the search space needed for initial beam establishment [26], [27]. In [26], the authors proposed a WiFi-based system that exploits angular information of the sub-6 GHz band to establish a directional mmWave link. The authors in [27] studied a deep learning-based mmWave beam prediction method, which employs a complex channel of each subcarrier as an input of a DNN. For the input of the DNN, we exploit CSI in terms of power-delay profiles (PDPs), and a detailed motivation of employing PDP is addressed in Section III-A. By adopting deep learning for beam selection, we can reduce the time overhead, which will be essential in 5G NR and 6G.

The rest of this paper is organized as follows. In Section II, we explain the system model and beam selection problem formulation. Section III explains our proposed deep learning-based beam selection method. Results of ray tracing-based simulations and prototype-based experiments are presented in Section IV, and Section V presents our conclusions.

II. SYSTEM MODEL AND PROBLEM FORMULATION

In this section, we explain our system and channel modelings.[1] Considering both sub-6 GHz and mmWave bands, we discuss the channel model of each band. Also, we formulate the beam selection problem that selects the mmWave beam with information of the sub-6 GHz channel.

A. CELLULAR NETWORKS AND CHANNEL MODELING

Consider the cellular networks that, as illustrated in Fig. 1, operate in both sub-6 GHz and mmWave. We assume gNBs support either sub-6 GHz or mmWave and UEs can be attached in both bands. Also, we assume each gNB, especially those operating in mmWave, is equipped with an array of antennas, and each UE has a single antenna. In practice, UEs are also usually designed with multiple antennas, and the beam selection procedure is performed on both the gNB side and the UE side. For simplicity, though, we assume single-antenna UEs and consider beam selection only on the gNB side. This way we can show the concept and feasibility of the proposed deep learning-based beam selection. Note that multiple-antenna UEs will be considered in our future work.

[1] Throughout this paper, we use upper and lower case boldface to describe matrix $\boldsymbol{A}$ and vector $\boldsymbol{a}$, respectively. The transpose and the Hermitian transpose of a matrix is notated as $(\cdot)^T$ and $(\cdot)^H$, respectively. $\mathrm{dg}(\boldsymbol{a})$ is a diagonal matrix whose entries are the elements of $\boldsymbol{a}$, and $\mathrm{Dg}(\boldsymbol{A})$ is a column vector whose elements are the diagonal entries of $\boldsymbol{A}$.

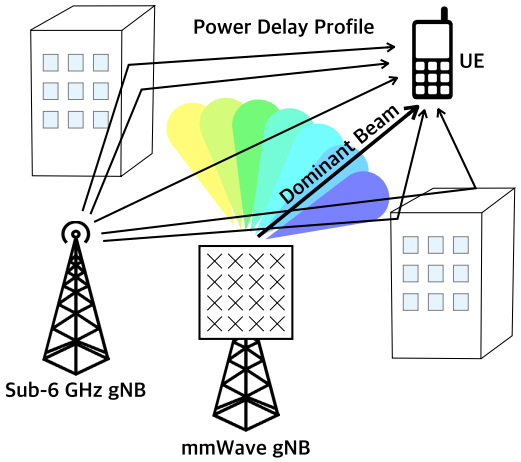

FIGURE 1. The system model with the sub-6 GHz and mmWave bands. A sub-6 GHz gNB is used for PDP estimation and a mmWave gNB tries to find the dominant beam. Note that sub-6 GHz and mmWave gNBs are deployed in different positions.

Basically, in this paper, we generate wireless channels with 3D ray tracing [30], the details of which are addressed in Section IV-A. From 3D ray tracing, we obtain channel parameters including power (or gain) P_m, delay τ_m, azimuth angle of arrival (AoA) θ_m^{AoA}, azimuth angle of departure (AoD) θ_m^{AoD}, zenith angle of arrival (ZoA) θ_m^{ZoA}, and zenith angle of departure (ZoD) θ_m^{ZoD}. The subscript m denotes that these are the parameters of the m-th ray. Note that channel parameters of mmWave and sub-6 GHz channels do not need to be the same.

1) mmWave CHANNEL MODEL

For the mmWave channel model, we employ the channel model presented in [31]. As noted above, we consider a multiple-input single-output (MISO) channel with gNBs equipped with uniform linear arrays (ULAs) of N antennas and UEs with isotropic antennas. Note that ULAs can be simply expanded to planar arrays. For simplicity, we assume that all antennas are single polarized, and both gNBs and UEs do not move, making the channels static. Also, we assume a narrowband channel model. Note that, considering OFDM systems in 5G NR, we can simply expand our discussion to a wideband system by modeling and calculating received power at multiple subcarriers. Then, the mmWave channel model between the gNB and the UE is obtained as

$$\boldsymbol{h}^{\text{mm}} = \begin{bmatrix} h_1^{\text{mm}} & h_2^{\text{mm}} & \cdots & h_N^{\text{mm}} \end{bmatrix}, \tag{1}$$

where the sub-channel of the n-th antenna element is modeled as

$$h_n^{\text{mm}} = \sum_{m=0}^{M-1} \sqrt{P_m} \exp\left(j\Phi_m^{\text{mm}}\right) F_{\text{TX}}^{\text{mm}}\left(\theta_m^{\text{ZoD}}, \phi_m^{\text{AoD}}\right) \times \exp\left(\frac{j2\pi (\boldsymbol{r}_m^{\text{TX}})^T \cdot \boldsymbol{d}_n^{\text{TX}}}{\lambda_0}\right) \tag{2}$$

for $1 \le n \le N$, where M is the number of rays, λ_0 is a wavelength of a carrier frequency, and $F_{\text{TX}}^{\text{mm}}(\cdot)$ is the field pattern of each mmWave transmit antenna element. $\boldsymbol{d}_n^{\text{TX}}$ is the 3×1 location vector of transmit antenna element n and

$$\boldsymbol{r}_m^{\text{TX}} = \begin{bmatrix} \sin(\theta_m^{\text{ZoD}})\cos(\phi_m^{\text{AoD}}) \\ \sin(\theta_m^{\text{ZoD}})\sin(\phi_m^{\text{AoD}}) \\ \cos(\theta_m^{\text{ZoD}}) \end{bmatrix}.$$

Φ_m^{mm} is the random phase of the m-th ray which is randomly generated with the uniform distribution $\mathcal{U}(-\pi, \pi)$.

2) SUB-6 GHz CHANNEL MODEL

Since we utilize the PDP of sub-6 GHz channels for mmWave beam selection, for the sub-6 GHz channel model, we simply assume a single-input single-output (SISO) channel with the tapped delay line (TDL) model [32]. Note that we can expand our discussion to a multiple-antenna system to increase PDP estimation accuracy. First, we calculate the complex channel coefficient of the m-th ray as

$$h_m^{\text{sub}} = \sqrt{P_m} e^{j\Phi_m^{\text{sub}}} F_{\text{TX}}^{\text{sub}}\left(\theta_m^{\text{ZoD}}, \phi_m^{\text{AoD}}\right), \tag{3}$$

where $F_{\text{TX}}^{\text{sub}}(\cdot)$ is the field pattern of a sub-6 GHz transmit antenna. Φ_m^{sub} is also the random phase of the m-th ray generated with $\mathcal{U}(-\pi, \pi)$. Note that Φ_m^{mm} and Φ_m^{sub} are independent. Then, since the true delay τ_m of h_m^{sub} does not coincide with the integer multiples of the sampling period t_s, we use a simple rounding and tap re-sampling method. The sampled time-domain channel $\boldsymbol{h}^{\text{sub}}$ is defined as

$$\boldsymbol{h}^{\text{sub}} = \begin{bmatrix} h^{\text{sub}}[0] & h^{\text{sub}}[1] & \cdots & h^{\text{sub}}[L-1] \end{bmatrix}^T, \tag{4}$$

where L is the length of the channel and $h^{\text{sub}}[\ell]$ is the ℓ-th tap of $\boldsymbol{h}^{\text{sub}}$ for $0 \le \ell \le L-1$. It is initialized as $h^{\text{sub}}[\ell] = 0$ for $0 \le \ell \le L-1$. After the initialization, for the m-th ray, we calculate the discretized delay index ℓ_m and the relative difference τ_m^{r} as

$$\ell_m = \text{floor}(\tau_m / t_s),$$
$$\tau_m^{\text{r}} = \tau_m / t_s - \ell_m.$$

Note that $0 \le \tau_m^{\text{r}} < 1$. For re-sampling, h_m^{sub} is split into two adjacent taps, and the two taps of $\boldsymbol{h}^{\text{sub}}$ in (4) are updated as

$$\tilde{h}^{\text{sub}}[\ell_m] = h^{\text{sub}}[\ell_m] + \sqrt{1-\tau_m^{\text{r}}} h_m^{\text{sub}},$$
$$\tilde{h}^{\text{sub}}[\ell_m + 1] = h^{\text{sub}}[\ell_m + 1] + \sqrt{\tau_m^{\text{r}}} h_m^{\text{sub}},$$

where $\tilde{h}^{\text{sub}}[\ell_m]$ and $\tilde{h}^{\text{sub}}[\ell_m + 1]$ are the updated taps. By repeating this for $h_1^{\text{sub}}, \cdots, h_M^{\text{sub}}$ and superposing them, we have the sampled time-domain channel $\boldsymbol{h}^{\text{sub}}$.

B. BEAM SELECTION PROBLEM FORMULATION

For beamforming, we simply adopt the discrete Fourier transform (DFT)-based codebook—a codebook widely adopted in 3GPP [33]. Denote a steering vector which is a column of the DFT matrix as

$$\boldsymbol{w}_b = \frac{1}{\sqrt{N}} \begin{bmatrix} 1 & e^{-j2\pi \cdot 1 \cdot b} & \cdots & e^{-j2\pi \cdot (N-1) \cdot b} \end{bmatrix}^T, \tag{5}$$

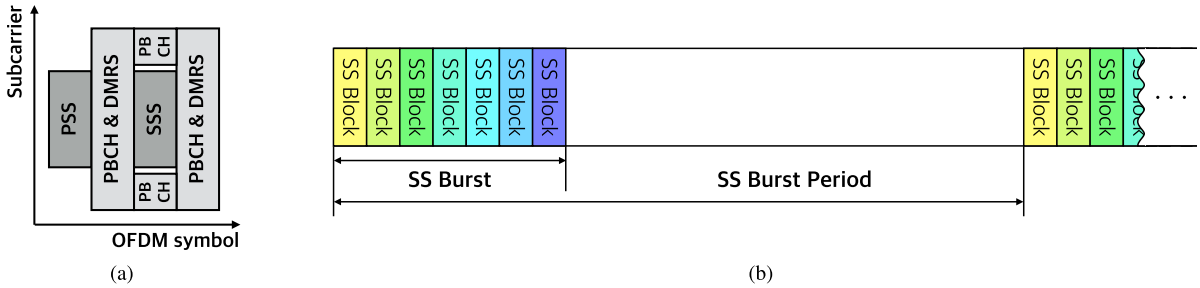

FIGURE 2. (a) The structure of an SS block. One SS block consists of four OFDM symbols. (b) A frame structure of an SS burst. Each SS block is used for each beam in Fig. 1, where the colors of SS blocks correspond to the beam colors.

where $0 \leq b \leq N-1$ is a beam index. Then, with the channel model in (1), the received mmWave signal y at the UE is modeled as

$$y = \boldsymbol{h}^{\mathrm{mm}} \boldsymbol{w}_b x + z, \tag{6}$$

where x is the transmitted signal from the gNB and z is the additive white Gaussian noise (AWGN) with a zero mean and variance of σ_z^2. Therefore, finding the optimal beam $\hat{b}$ can be expressed as

$$\hat{b} = \arg\max_b ||\boldsymbol{h}^{\mathrm{mm}} \boldsymbol{w}_b||. \tag{7}$$

III. DEEP LEARNING-BASED BEAM SELECTION

In this section, we first introduce the conventional beam selection in the 5G NR standard and the motivation of our proposed deep learning-based beam selection method. Then, we describe the proposed method with two parts: CSI acquisition and beam selection. First, we introduce how we obtain CSI based on the 3GPP NR standard, and explain the DNN structure and beam selection method.

A. CONVENTIONAL BEAM SELECTION IN 5G NR AND THE MOTIVATION FOR THE DEEP LEARNING-BASED BEAM SELECTION

In the 5G NR standard, the main procedure of beam selection is beam sweeping, which transmits a set of pre-defined beams, so-called synchronization signal blocks (SS blocks) [34], to cover spatial area. Among the predefined spatial directions, beam sweeping exhaustively searches for its best beam. As illustrated in Fig. 2(a), an SS block consists of four OFDM symbols of primary synchronization signal (PSS), secondary synchronization signal (SSS), physical broadcast channel (PBCH), and demodulation reference signal (DMRS). A set of SS blocks within beam sweeping is referred to as an SS burst, as illustrated in Fig. 2(b). The length of SS burst is a maximum of 5 ms and each SS burst may have SS blocks up to 64 blocks in the mmWave band [35]. Each SS block is used for a specific beam for beam sweeping as SS blocks in Fig. 2(b) are allocated to beams in Fig. 1 with corresponding colors.

However, even in the eMBB scenario, the initial beam establishment time overhead of 5 ms may be too long. Similar to prior works [18]–[23], we adopt the concept of deep learning to reduce the search space of beam sweeping. An important thing is deciding what to exploit as the input of the DNN. Even though other components such as GPS [18]–[20] or LIDAR [21] can provide additional information, it is followed by extra costs, and hard for the 5G NR standard to adopt and rely on them. Therefore, in this paper, we employ what can be obtained via conventional wireless transceivers either sub-6 GHz or mmWave. From the insight that the beams we considered are formed in the angular domain, it is natural to employ channel characteristics such as AoD or PDP. However, the main obstacle is that mmWave channel characteristics are impossible to obtain before mmWave initial beam establishment.

The solution presented in this paper is to employ the channel characteristics of the sub-6 GHz band. It is widely known that the sub-6 GHz and mmWave channels have very different characteristics, but recently some results show there are strong angular and temporal correlations among mmWave and sub-6 GHz channels in certain conditions [36]. However, to employ angular information for a deep learning-based beam selection [23], there are several obstacles. First, to estimate angular information accurately, a size of an antenna array needs to be large [37]. However, since the antenna array size is limited in practical scenarios, so is the angular estimation performance. Also, the number of multipaths (defined as M) needs to be fixed for the estimation algorithms such as the MUSIC algorithm [38] and the DNN structure introduced in [23]. It does not fit for practical environments where M varies.

What we pay attention to is that in a cell-specific manner with given environments, channel characteristics such as PDP can be considered as a fingerprint for UE position. In other words, with a given gNB and environment, PDP can specify a UE's position. Therefore, even locations of mmWave and sub-6 GHz gNBs are different, we believe the sub-6 GHz PDP can be used for mmWave beam selection. Moreover, as sub-6 GHz cells cover macro areas while mmWave cells support small areas with high throughput, it is reasonable to assume the UE, which tries to establish a mmWave link, is connected to the sub-6 GHz networks.

B. 3GPP NR-BASED CSI ACQUISITION

In 3GPP NR, there are two special reference signals defined for channel sounding: a CSI reference signal (CSI-RS)

for downlink and a sounding reference signal (SRS) for uplink [34]. Let us consider a downlink CSI-RS is exploited for CSI acquisition for beam selection. Recalling that the sub-6 GHz channel, which is exploited for CSI acquisition, is assumed SISO, a single-port CSI-RS should be employed. However, a single-port CSI-RS occupies a resource element (RE) within a resource block (RB). This means that out of 84 REs only one RE is used for estimation. This may lead to performance degradation of CSI estimation. Also, to estimate CSI via downlink with reference signals, the UE has to feed the estimated CSI back to the gNB or the central unit for training or beam selection. This incurs an accuracy loss of CSI and feedback overhead. Therefore, in this paper, we employ an uplink SRS for CSI acquisition.

An SRS is generated by allocating an extended Zadoff-Chu (ZC) sequence to REs [34]. The ZC sequence is defined as

$$x_q[k] = e^{-j\frac{\pi qk(k+1)}{N_{\mathrm{ZC}}}}$$

for $0 \leq k \leq N_{\mathrm{ZC}} - 1$, where N_{ZC} is the length of the ZC sequence and q is the root index of the sequence. In 5G NR, N_{ZC} is given by the largest prime number which is smaller than the length of the reference signal sequence N_{RS}. One of the key properties of the ZC sequences is the constant amplitude zero autocorrelation (CAZAC) property. Also, the DFT of a ZC sequence is a ZC sequence. Because $N_{\mathrm{ZC}} < N_{\mathrm{RS}}$, the ZC sequence $x_q[k]$ is cyclically extended to generate the SRS sequence $\boldsymbol{x}_{\mathrm{SRS}}$ as

$$\begin{aligned} \boldsymbol{x}_{\mathrm{SRS}} &= \begin{bmatrix} x_{\mathrm{SRS}}[0] & \cdots & x_{\mathrm{SRS}}[N_{\mathrm{RS}}-1] \end{bmatrix}^T, \quad (8) \\ x_{\mathrm{SRS}}[k] &= x_q[k \bmod N_{\mathrm{ZC}}]. \end{aligned}$$

Then, in frequency domain, $\boldsymbol{x}_{\mathrm{SRS}}$ is allocated on every second or fourth subcarrier, called comb-2 and comb-4, respectively. Let $\mathcal{K}_{\mathrm{SRS}}$ denotes the indices of the allocated subcarriers and $|\mathcal{K}_{\mathrm{SRS}}| = N_{\mathrm{RS}}$. Also, in the time domain, it spans one, two, or four consecutive symbols that are mapped within the last six symbols of a slot. These multiple SRS symbols allow coverage extension and increased sounding capacity.

Exploiting the SRS, we estimate the PDP of the channels. Consider an OFDM system with the fast Fourier transform (FFT) size N_{FFT} and the number of used subcarriers K. For example, with a sampling rate of 30.72 MHz, a system with the 20 MHz bandwidth is defined with $N_{\mathrm{FFT}} = 2048$ and $K = 1272$ in 5G NR. Note that $K < N_{\mathrm{FFT}}$ in order to control adjacent channel interference. However, $N_{\mathrm{FFT}} - K$ null subcarriers cause serious performance degradation to the DFT-based channel estimation, the so-called the edge effect.

In this paper, we apply the PDP estimation method introduced in [39], a work in which the authors considered the edge effect to be caused by limited pilot allocation. Omitting the detail processes of cyclic prefix (CP)-OFDM systems such as FFT, CP insertion, synchronization, CP removal and inverse FFT (IFFT), the OFDM system that transmits the SRS in (8) can be represented as

$$\boldsymbol{y}_{\mathrm{SRS}}[n_{\mathrm{s}}] = \mathrm{dg}(\boldsymbol{x}_{\mathrm{SRS}})\boldsymbol{F}_{\mathrm{SRS}}\boldsymbol{h}^{\mathrm{sub}} + \boldsymbol{z}[n_{\mathrm{s}}],$$

where $\boldsymbol{x}_{\mathrm{SRS}}$, $\boldsymbol{y}_{\mathrm{SRS}}[n_{\mathrm{s}}]$, and $\boldsymbol{z}[n_{\mathrm{s}}]$ are the $N_{\mathrm{RS}} \times 1$ transmit signal, receive signal, and AWGN vector with a zero mean and variance of σ_z^2, respectively. $1 \leq n_{\mathrm{s}} \leq N_{\mathrm{s}}$ denotes an OFDM symbol index, and N_{s} is the number of used symbols. We assume that same $\boldsymbol{x}_{\mathrm{SRS}}$ is used for N_{s} symbols. $\boldsymbol{F}_{\mathrm{SRS}}$ is an $N_{\mathrm{RS}} \times L$ matrix consists of the (k, ℓ)-th entries of the DFT matrix $1/\sqrt{N_{\mathrm{FFT}}}\exp(-j2\pi k\ell/N_{\mathrm{FFT}})$ where $k \in \mathcal{K}_{\mathrm{SRS}}$ and $0 \leq \ell \leq L-1$. Then, by using the regularized least squares (RLS) estimation, the estimated channel with a fixed length of L is obtained as

$$\boldsymbol{W}_{\mathrm{R}} = \left(\boldsymbol{F}_{\mathrm{SRS}}^H\boldsymbol{F}_{\mathrm{SRS}} + \varepsilon\boldsymbol{I}_L\right)^{-1}\boldsymbol{F}_{\mathrm{SRS}}^H\mathrm{dg}(\boldsymbol{x}_{\mathrm{SRS}})^{-1}, \quad (9)$$

$$\hat{\boldsymbol{h}}^{\mathrm{sub}}[n_{\mathrm{s}}] = \boldsymbol{W}_{\mathrm{R}}\boldsymbol{y}_{\mathrm{SRS}}[n_{\mathrm{s}}], \quad (10)$$

where $\varepsilon = 0.001$ is a small regularization parameter, and $\boldsymbol{I}_L$ is an $L \times L$ identity matrix. Note that the aforementioned edge effect can also be explained by the fact that $\boldsymbol{F}_{\mathrm{SRS}}^H\boldsymbol{F}_{\mathrm{SRS}}$ in (9) is ill-conditioned. Then, the PDP of the estimated channel in (10) is derived as

$$\mathbb{E}\left[\hat{\boldsymbol{h}}^{\mathrm{sub}}\left(\hat{\boldsymbol{h}}^{\mathrm{sub}}\right)^H\right] = \boldsymbol{W}\boldsymbol{R}_{\boldsymbol{h}}\boldsymbol{W}^H + \sigma_z^2\boldsymbol{W}_{\mathrm{R}}\boldsymbol{W}_{\mathrm{R}}^H, \quad (11)$$

where

$$\begin{aligned} \boldsymbol{W} &= \left(\boldsymbol{F}_{\mathrm{SRS}}^H\boldsymbol{F}_{\mathrm{SRS}} + \varepsilon\boldsymbol{I}_L\right)^{-1}\boldsymbol{F}_{\mathrm{SRS}}^H\boldsymbol{F}_{\mathrm{SRS}}, \\ \boldsymbol{R}_{\boldsymbol{h}} &= \mathbb{E}\left[\boldsymbol{h}^{\mathrm{sub}}(\boldsymbol{h}^{\mathrm{sub}})^H\right]. \end{aligned}$$

To avoid the distortion of $\boldsymbol{W}$, the distortion matrix $\boldsymbol{T}$ is defined as follows:

$$\begin{aligned} \boldsymbol{t}_\ell &= \mathrm{Dg}\left(\boldsymbol{W}\mathrm{dg}(\boldsymbol{u}_\ell)\boldsymbol{W}^H\right), \\ \boldsymbol{T} &= \begin{bmatrix} \boldsymbol{t}_1 & \boldsymbol{t}_2 & \cdots & \boldsymbol{t}_L \end{bmatrix}, \end{aligned}$$

where $\boldsymbol{u}_\ell$ is an $L \times 1$ unit vector with the ℓ-th entry being one and otherwise zeros. Then, we can obtain the PDP with SRS as

$$\boldsymbol{p}[n_{\mathrm{s}}] = \boldsymbol{g}[n_{\mathrm{s}}] - \sigma_z^2\boldsymbol{w}, \quad (12)$$

where $\boldsymbol{g}[n_{\mathrm{s}}]$ and $\boldsymbol{w}$ are defined as

$$\begin{aligned} \boldsymbol{g} &= \boldsymbol{T}^{-1}\mathrm{Dg}\left(\hat{\boldsymbol{h}}^{\mathrm{sub}}[n_{\mathrm{s}}]\left(\hat{\boldsymbol{h}}^{\mathrm{sub}}[n_{\mathrm{s}}]\right)^H\right), \\ \boldsymbol{w} &= \boldsymbol{T}^{-1}\mathrm{Dg}\left(\boldsymbol{W}_{\mathrm{R}}\boldsymbol{W}_{\mathrm{R}}^H\right). \end{aligned}$$

Since we can employ multiple symbols of SRS, the initial estimated PDP is calculated as

$$\boldsymbol{p}_0 = \frac{1}{N_{\mathrm{s}}}\sum_{n_{\mathrm{s}}=1}^{N_{\mathrm{s}}}\boldsymbol{x}^+(\boldsymbol{p}[n_{\mathrm{s}}]), \quad (13)$$

where $\boldsymbol{x}^+(\cdot)$ is an operator that replaces negative entries to zero. Then, to mitigate the effect of residual noise, the average of residual noise at the zero-taps of $\boldsymbol{p}$ is estimated. First, for $1 \leq \ell \leq L$, the zero-tap can be detected as

$$t^\ell = \begin{cases} 1, & p_0^\ell < \beta_{\mathrm{th}}, \\ 0, & \text{otherwise}, \end{cases}$$

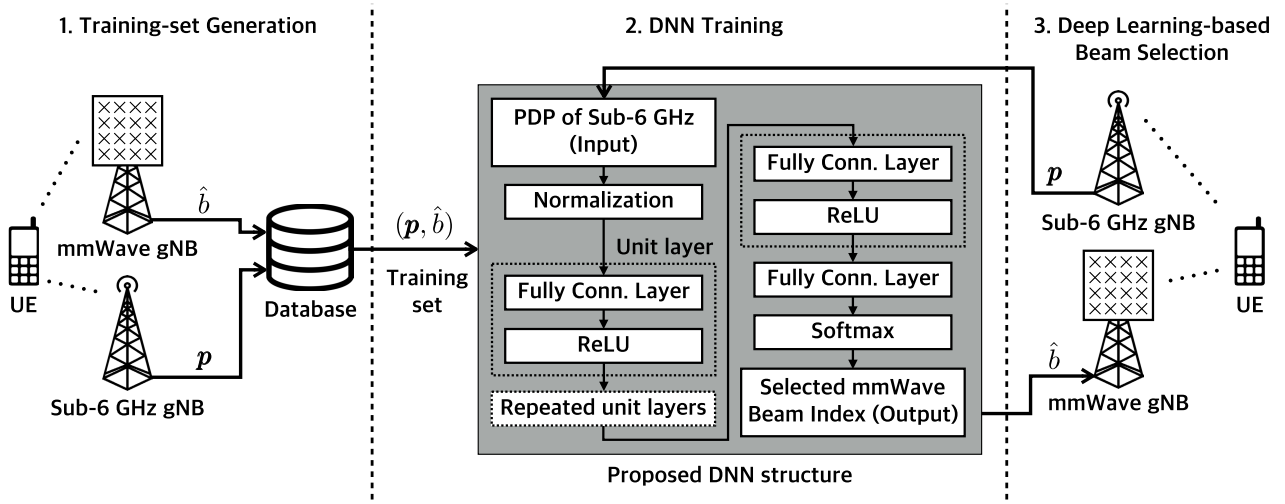

FIGURE 3. A schematic of the training-set generation, the DNN training, and beam selection of the proposed deep learning-based beam selection method. A gray box shows the proposed structure of the DNN. A unit layer consists of the fully connected layer and the ReLU layer, and the DNN is constructed by repeating a number of unit layers.

where p_0^ℓ is the ℓ-th element of $\boldsymbol{p}_0$ and $\beta_{\text{th}} = \frac{1}{L}\sum_{\ell=1}^{L} p_0^\ell$ is defined as a threshold value for zero-tap detection. Then, the average of residual noise is estimated as

$$n_{\text{avg}} = \frac{1}{\sum_{\ell=1}^{L} t^\ell} \sum_{\ell=1}^{L} t^\ell p_0^\ell. \tag{14}$$

By mitigating the noise effect, the final estimated PDP is obtained as

$$\boldsymbol{p} = \boldsymbol{x}^+(\boldsymbol{p}_0 - n_{\text{avg}}). \tag{15}$$

C. DEEP LEARNING-BASED BEAM SELECTION

The proposed deep learning-based beam selection consists of three parts: a training-set generation part, a DNN training part, and a beam selection part. Fig. 3 shows a schematic of the proposed beam selection. First, considering supervised learning, we need to collect a labeled input and output data set. For the training-set generation, we adopt the conventional exhaustive search-based beam sweeping. Even though the proposed beam selection works properly, for backward compatibility, the 5G NR standard needs to provide the conventional beam sweeping as the mandatory method and the proposed one as the optional. Like the proposed beam selection, the training set is generated in a separate-gNB manner. Each mmWave gNB collects labeled data—a pair of the optimal beam index $\hat{b}$ and the estimated PDP $\boldsymbol{p}$—when it establishes a link with a UE. Note that the sub-6 GHz gNB estimates $\boldsymbol{p}$ and reports it to the mmWave gNB. Then, after the database of the gNB collects enough amount of data, the DNN starts training.

To explain the DNN training, we need to explain our DNN structure first.

In this paper, to determine which beam should be chosen, we adopt the DNN constructed with the fully connected layers. As illustrated in Fig. 3, the DNN consists of $L_{\text{H}}+2$ layers including an input layer, L_{H} hidden layers, and an output layer. First, the input layer, the size of which is L, gets the sub-6 GHz PDP vector $\boldsymbol{p}$ in (15). After that, as each element of $\boldsymbol{p}$ has a very different scale—decreasing exponentially in general—we re-scale the n-th element of $\boldsymbol{p}$ as

$$\bar{\boldsymbol{p}}[n] = \boldsymbol{p}[n]^{0.1}. \tag{16}$$

Then, since $\boldsymbol{p}[n] \in [0, 1]$, the range maintains $\bar{\boldsymbol{p}}[n] \in [0, 1]$, and a very small value is scaled up. For example, $\boldsymbol{p}[n] = 10^{-10}$, which can be measured considering the transmit power of 23 dBm and the noise level of -90 dBm, is re-scaled to $\bar{\boldsymbol{p}}[n] = 0.1$. This prevents the weights of the DNN from becoming too large. The exponent value of 0.1 is determined empirically. Each hidden layer is made up of the fully connected layer with rectified linear units (ReLU) as the activation function. The number of hidden layers (L_{H}) and the size of each layer will be given in Section IV-B. Returning the probability of each beam, the output layer is designed with the size of the number of candidate beams (N) and the softmax function as its activation function. We employ the cross entropy as the cost function and adopt the Adam optimization algorithm for training the DNN. To avoid overfitting, we apply dropout with a rate of 0.1.

Since the DNN returns the possibilities of beam indices, the simplest way for beam selection is to select the most likely one. In this way, we can select the beam by just transmitting one slot for sub-6 GHz SRS with 15 kHz subcarrier spacing (1 ms) and one mmWave SS block (35.68 μs; 4 OFDM symbols). Recalling the maximum length of an SS burst is 5 ms, we can reduce time overhead by up to 79.3 %. However, in certain environments, the accuracy of selecting the most probable beam may not be high enough. Therefore, we propose the beam selection method that chooses the k highest outputs and performs beam sweeping among these k candidates. In this paper, we denote this method as Bk-selection,

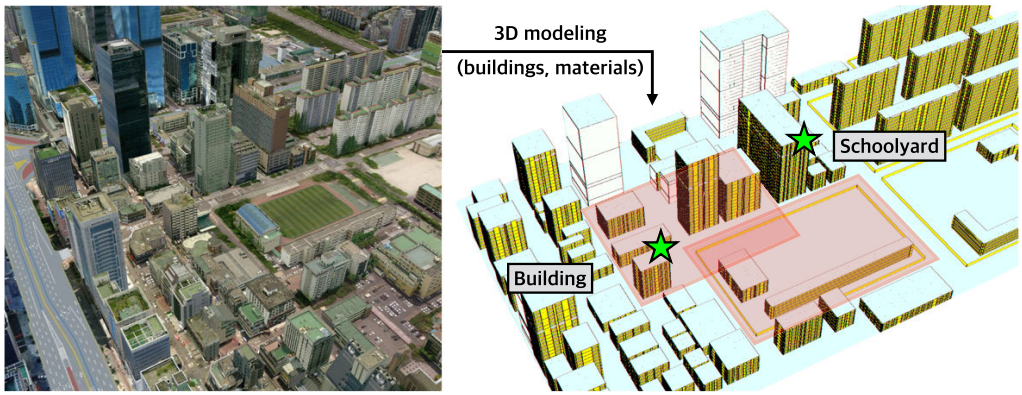

FIGURE 4. The real 3D map of the Gangnam station area in Seoul, Korea (left) and our 3D map modeling for ray tracing (right). The green stars indicate where gNBs are placed in the building area and the schoolyard area.

TABLE 1. Parameters for performance evaluation.

Parameters		Values		
mmWave carrier frequency		28 GHz		
The number of beams N		16, 64		
Antenna-element spacing		0.5 λ_0		
Sub-6 GHz carrier frequency		3.5 GHz		
Sub-6 GHz signal bandwidth (MHz)		20	40	50
FFT size N_{FFT}		2048	4096	4096
Used subcarrier K		1272	2592	3240
Sampling rate (MHz)		30.72	61.44	61.44
CP length (or channel length) L		160	320	320
Vertical 3 dB beamwidth $\theta_{3\text{dB}}$		65°		
Horizontal 3 dB beamwidth $\phi_{3\text{dB}}$		65°		
Vertical side-lobe attenuation SLA_{v}		30 dB		
Maximum attenuation $A_{\max}$		30 dB		
Building area	Downtilt angle	90°		
	Bearing angle	15°		
	The number of UEs	51200		
	Height of the gNB	33 m		
Schoolyard area	Downtilt angle	270°		
	Bearing angle	35°		
	The number of UEs	55640		
	Height of the gNB	64.5 m		
UE grid spacing		0.5 m		
Transmit power		23 dBm		
Thermal noise		-100 dBm		

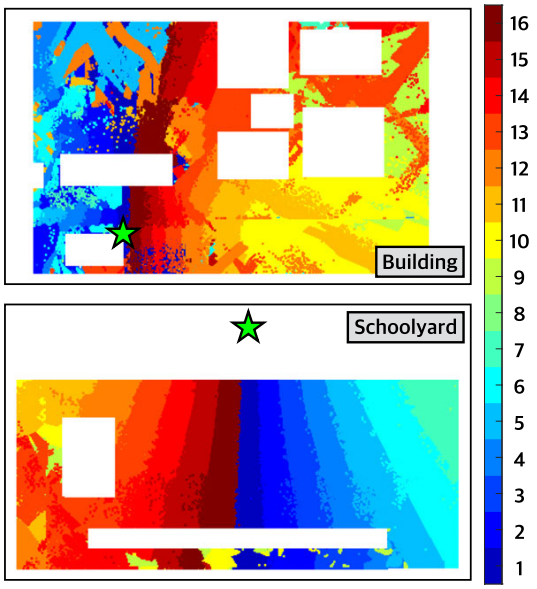

FIGURE 5. The distribution of the optimal beam indices of the schoolyard area (top) and the building area (bottom) where $N = 16$. The color bar shows beam indices 1 to 16, and the white areas are buildings. The green stars indicate where gNBs are placed.

which makes B1-selection as a one-shot selection. Note that as k increases, the time overhead of Bk-selection increases.

IV. PERFORMANCE EVALUATION

In this section, we evaluate the proposed deep learning-based beam selection. First, we explain the data set generation via the 3D ray-tracing tool. We generate wireless channels with 5G NR parameters and a 3D map of the real environment. Then, with the proposed DNN, we evaluate the performance of beam selection. Also, we verified the proposed beam selection with the 5G NR prototype.

A. 3D RAY TRACING-BASED DATA SET GENERATION

As explained in Section III-C, we first generate channel parameters via 3D ray tracing [30]. For 3D ray tracing, we used Wireless System Engineering (WiSE), the 3D ray-tracing tool developed by Bell Labs [40]. We first made the 3D map, as shown in Fig. 4, of the Gangnam station area in Seoul. This 3D map reflects the real sizes of buildings and materials such as concrete and glass. In the Gangnam station area, we selected two area types: a building area and a schoolyard area. The former is to consider a case having many reflections, while a latter with fewer. We, then, deploy gNBs on the roofs of buildings in both areas, as illustrated in Fig. 4. Since we consider the two different bands, mmWave gNBs are deployed 1 m next to sub-6 GHz gNBs. UEs are assumed to be on the outdoor ground (1 m above from the ground).

We assumed that both sub-6 GHz and mmWave gNBs are equipped with directional antennas with the pattern defined in [31]. For $\theta \in [0°, 180°]$ and $\phi \in [-180°, 180°]$, vertical

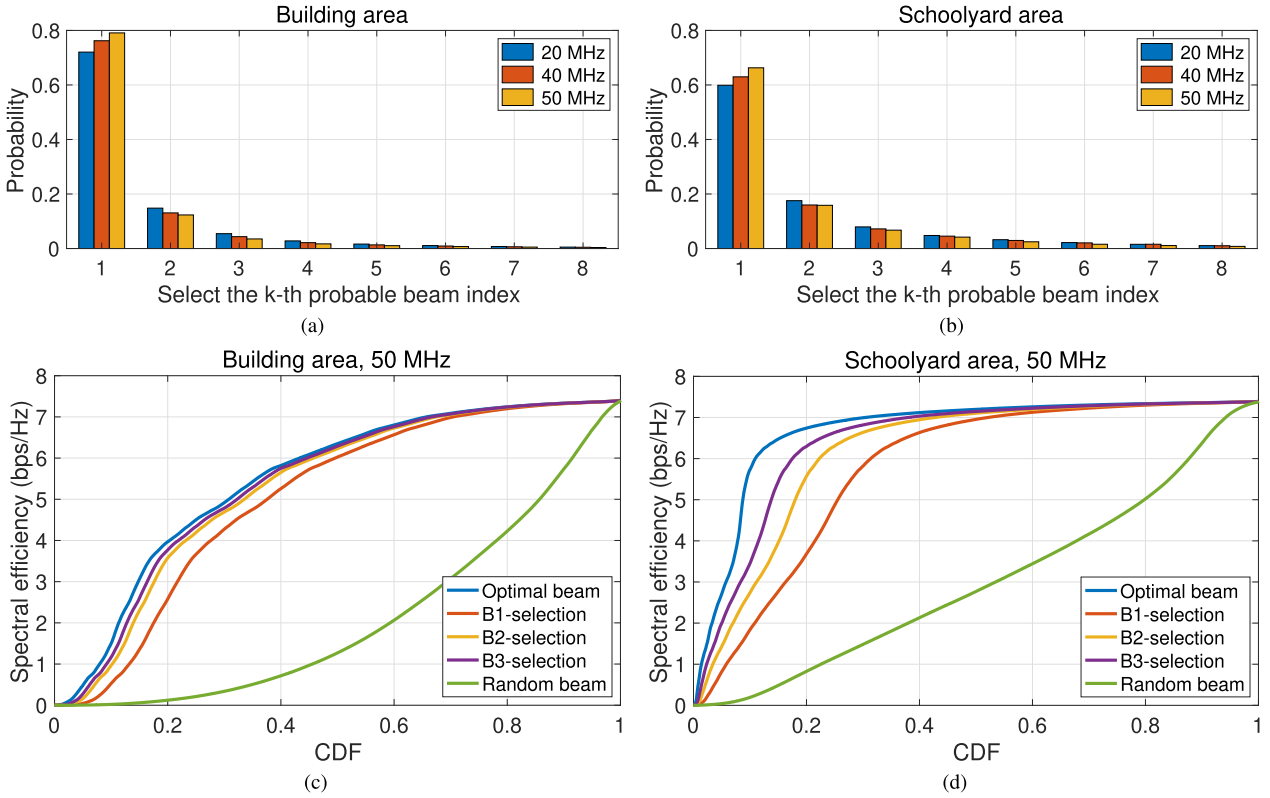

FIGURE 6. (a) and (b) are the beam selection accuracy of the k-th probable beam index with $N = 16$ and sub-6 GHz bandwidths of 20, 40, and 50 MHz in the building area and the schoolyard area, respectively. (c) and (d) are the CDF of spectral efficiency with sub-6 GHz bandwidth of 50 MHz in the building area and the schoolyard area, respectively. The results include spectral efficiency with the optimal beam, B1-, B2-, and B3-selection beam, and random beam.

and horizontal attenuations are defined as

$$A_{\mathrm{v}}(\theta) = \min\left(12\left(\frac{\theta - 90^{\circ}}{\theta_{3\mathrm{dB}}}\right)^2, SLA_{\mathrm{v}}\right),$$

$$A_{\mathrm{h}}(\phi) = \min\left(12\left(\frac{\phi}{\phi_{3\mathrm{dB}}}\right)^2, A_{\max}\right),$$

where $\theta_{3\mathrm{dB}}$ and $\phi_{3\mathrm{dB}}$ are vertical and horizontal 3 dB beamwidth, respectively. SLA_{v} and $A_{\max}$ are vertical side-lobe attenuation and maximum attenuation, respectively. Then, the antenna pattern is obtained as

$$G(\theta, \phi) = G_{\max} - \min\left(A_{\mathrm{v}}(\theta) + A_{\mathrm{h}}(\phi), A_{\max}\right), \quad (17)$$

where $G_{\max}$ is a maximum directional gain. Then, we substitute the antenna pattern into the channel model in (2) and (3) as $F_{\mathrm{TX}}^{\mathrm{mm}}(\theta, \phi) = F_{\mathrm{TX}}^{\mathrm{sub}}(\theta, \phi) = \sqrt{G(\theta, \phi)}$. For simplicity, each UE is equipped with an isotropic antenna. Table 1 provides all the parameters including bearing angles and downtilt angles of the gNBs.

With the channel parameters, we generated the mmWave and sub-6 GHz channels as explained in Section II. We, then, calculated the estimated PDPs $\boldsymbol{p}$ in (15) and the corresponding optimal beam indices $\hat{b}$ as (7) with the number of beams $N = 16, 64$. Considering small scale fading, represented by the random phase Φ_m in (2) and (3), we generated 100 pairs of $(\boldsymbol{p}, \hat{b})$ for each UE position. Therefore, the sizes of the data set are 5.12M and 5.564M for the building area and the schoolyard area, respectively. We divided the data set into the training set and the validation set by randomly dividing UE positions with a ratio of 70% and 30%, respectively. In Section IV-B, these training and validation sets are used for performance evaluations. Fig. 5 shows how the optimal beam indices $\hat{b}$ are distributed in the building area and the schoolyard area. We can observe that the optimal beam indices are highly spatially correlated.

B. BEAM SELECTION PERFORMANCE

First, we constructed the simple DNN and evaluated the beam selection performance with different values of sub-6 GHz bandwidth. The DNN has three hidden layers ($L_{\mathrm{H}} = 3$); their sizes are 1024, 512, and 256, respectively. As listed in Table 1, we investigated with the bandwidths of 20, 40, and 50 MHz. Note that as the bandwidth changes, other parameters such as an FFT size, the number of used subcarriers, a sampling rate, and a channel length also change.

We first evaluated the performance of the proposed beam selection method in terms of accuracy with the number of beams $N = 16$. Fig. 6(a) and (b) show, respectively, the probability that the k-th probable beam index (or the k-th highest output of the DNN) is the optimal beam index in the building

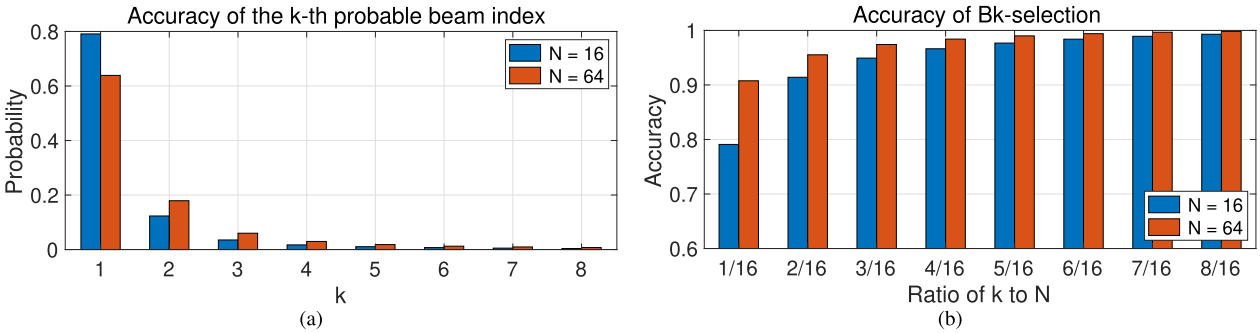

FIGURE 7. (a) and (b) are the accuracy of the k-th probable beam index and Bk-selection, respectively, with $N = 16,\ 64$ and the bandwidth of 50 MHz in the building area. (b) shows the results with the same ratio of k to N, i.e. $(k, N) = (1, 16)$ and $(4, 64)$.

area and the schoolyard area. Note that it is the probability mass function (PMF) of the accuracy of Bk-selection. In the building area, the optimal beam is selected by one shot with the probabilities of 0.72, 0.76, and 0.79 when the sub-6 GHz bandwidths are 20, 40, and 50 MHz, respectively. On the other hand, in the schoolyard area, the accuracies of one-shot beam selection are 0.60, 0.63, and 0.66 with the sub-6 GHz bandwidths of 20, 40, and 50 MHz, respectively. From this result, we can observe two trends. First, the proposed method shows better performance with the wider bandwidth of the sub-6 GHz channel. The reason is that the sampling rate of 40 and 50 MHz systems is higher than that of 20 MHz systems. This means the PDP $\boldsymbol{p}$ can be obtained with a higher resolution and the DNN can have more input. The disadvantage of narrow sub-6 GHz bandwidth can be overcome by the Bk-selection. For example, by selecting the beam among three candidates, the accuracies are 0.92, 0.93, and 0.95 in the building area with the sub-6 GHz bandwidths of 20, 40, and 50 MHz, respectively. Second, the proposed method works more accurately in the building area than in the schoolyard area. Since the wireless channels in the building area have more rays and reflections, they can give more information to the DNN. In other words, the PDPs, in the building area, have more non-zero elements than those in the schoolyard area.

Fig. 6(c) and (d) show the cumulative distribution function (CDF) of spectral efficiency with the sub-6 GHz bandwidth of 50 MHz in the building area and the schoolyard area, respectively. To calculate the spectral efficiency, we calculated signal-to-noise ratio (SNR) and applied the modulation and coding method in 5G NR. Note that the spectral efficiency does not exceed 7.4, which is the maximum spectral efficiency in 5G NR. In the building area, as shown in Fig 6(c), the mean values of spectral efficiency are 5.49, 5.04, 5.31, 5.39, and 2.12 with the optimal beam, B1-, B2-, and B3-selection, and random beam, respectively. The result shows that even the B1-selection performs 92 % compared to the optimal selection in terms of average spectral efficiency. Also, in the schoolyard area, the average spectral efficiency of B1-, B2-, and B3-selection are 86 %, 93 %, and 96 % compared to the optimal beam, respectively. However, in terms of 20-percentile, the spectral efficiencies of B1-selection are only 65 % and 55 % in the building area and the schoolyard area, respectively. Therefore, to support these users, B3-selection can be employed and the performances increase up to 95 % and 93 % comparing to the optimal selection, respectively.

To evaluate the performance of the case that uses all the possible SS blocks for the conventional beam sweeping, we also simulated with the same parameters but $N = 64$. Fig. 7(a) shows the accuracy of the k-th probable beam index with $N = 16,\ 64$ and the sub-6 GHz bandwidth of 50 MHz in the building area. We observed that the performance of B1-selection degrades as N increases. It is obvious because it is hard to pick the optimal beam among more beams. However, as shown in Fig. 7(b), considering the same ratio of k to N, the accuracy of Bk-selection with $N = 64$ is better than that with $N = 16$. For example, the accuracies are 0.91 and 0.79 with $(k, N) = (4, 64)$ and $(1, 16)$, respectively. Therefore, we confirmed that the proposed method also works properly with a large number of beams.

Further, we tested the proposed method with various sizes of data sets. As it is not feasible to expect the data set to be collected in all grids, we simulated the proposed method with a small portion of the whole data set. We randomly selected 20 %, 40 %, 60 %, 80 %, and 100 % of the data set with $N = 16$. Note that this data includes the training and validation sets, which means if we select 20 % of the whole data, the training and validation sets are 14 % and 6 % of the data, respectively. Fig. 8 shows the results with the sub-6 GHz bandwidth of 50 MHz in both areas. Fig. 8(a) and (b) show, respectively, the accuracy of the k-th probable beam index to be the optimal index in the building area and the schoolyard area. We observed that, as the size of the data set decreases, beam selection performances degrades. For example, the performances of B1-selection with 20 % of the data set are degraded 13 % and 11 %, respectively, compared to those performances using the whole data set in the building area and the schoolyard area.

C. PROTOTYPE VALIDATION

To validate the performance of the proposed deep learning-based beam selection, we did an over-the-air experiment with

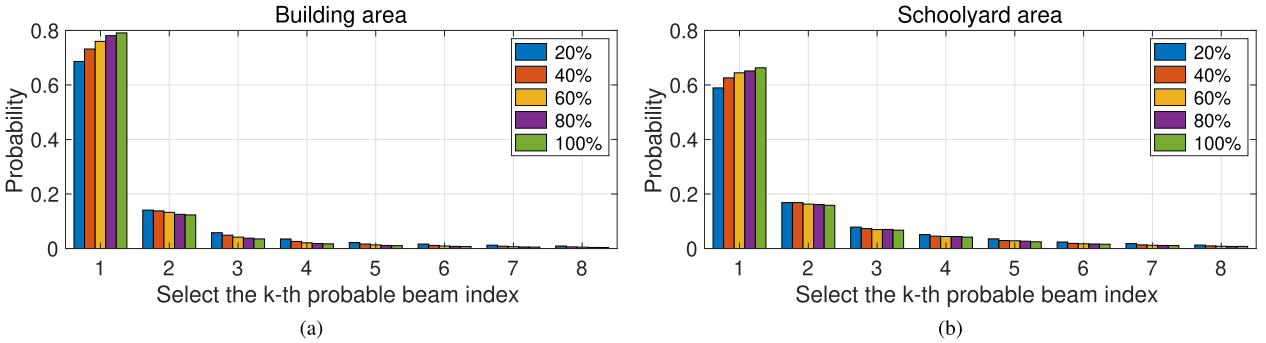

FIGURE 8. (a) and (b) are the beam selection accuracy of the k-th probable beam index with $N = 16$ and sub-6 GHz bandwidth of 50 MHz in the building area and the schoolyard area, respectively. To investigate the effect of the data size, we simulated with 20 %, 40 %, 60 %, 80 %, and 100 % of the whole data.

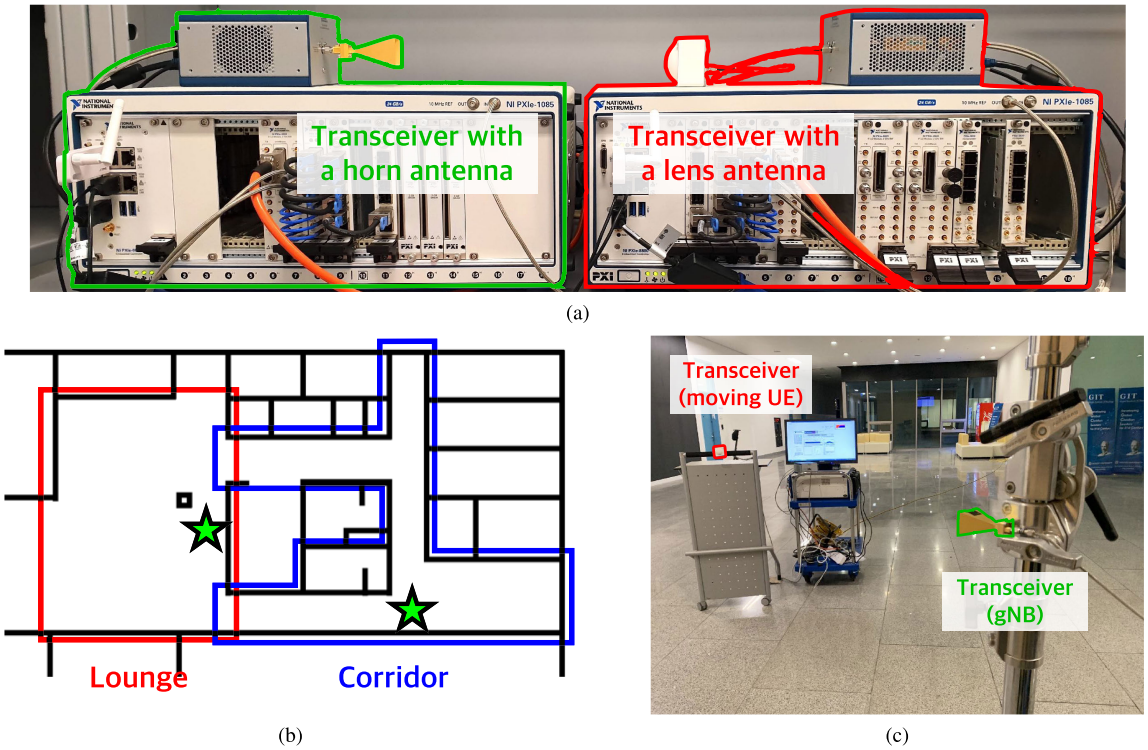

FIGURE 9. (a) The setup of the transceiver with the horn antenna and the transceiver with the lens antenna. (b) The regions of interest of lounge (red) and corridor (blue) scenarios. The green stars indicate where the gNB-like transceiver was placed. (c) The picture of experiment setup in Veritas C, Yonsei University.

our mmWave prototype. As shown in Fig. 9(a), we designed the mmWave transmitter and receiver with the software-defined radios (SDR) of National Instruments (NI). Both transmitter and receiver are equipped with chassis (NI PXIe-1085), controllers (NI PXIe-8880), and local oscillator (LO)/intermediate frequency (IF) modules (NI PXIe-3620). Also, the transmitter is equipped with an up-converter (NI mmRH-3642) and a horn antenna,[2] and the receiver is equipped with a field-programmable gate array (FPGA) module (NI PXIe-7976R), a down-converter (NI mmRH-3652), and a lens antenna [41], [42]. With the mmWave prototype, we transmitted CP-OFDM signals with a carrier frequency of 28.5 GHz and bandwidth of 800 MHz, and measured the received powers at the receiver.

We experimented in two scenarios: a lounge and a corridor. First, as shown in Fig. 9(b), we determined the regions of interest of both scenarios. We placed the transmitter, which works as a gNB in our experiments, as green star-marked in Fig. 9(b). To simplify experiments, we constructed transmit beams by rotating the directional transmit antenna. In this paper, we used 5 beams to cover 180° by rotating 45° for each beam. Then, moving the receiver, we measured the received power of each transmit beam at every point with

[2]SAR-2013-28-S2: https://www.sagemillimeter.com/content/datasheets/SAR-2013-28-S2.pdf

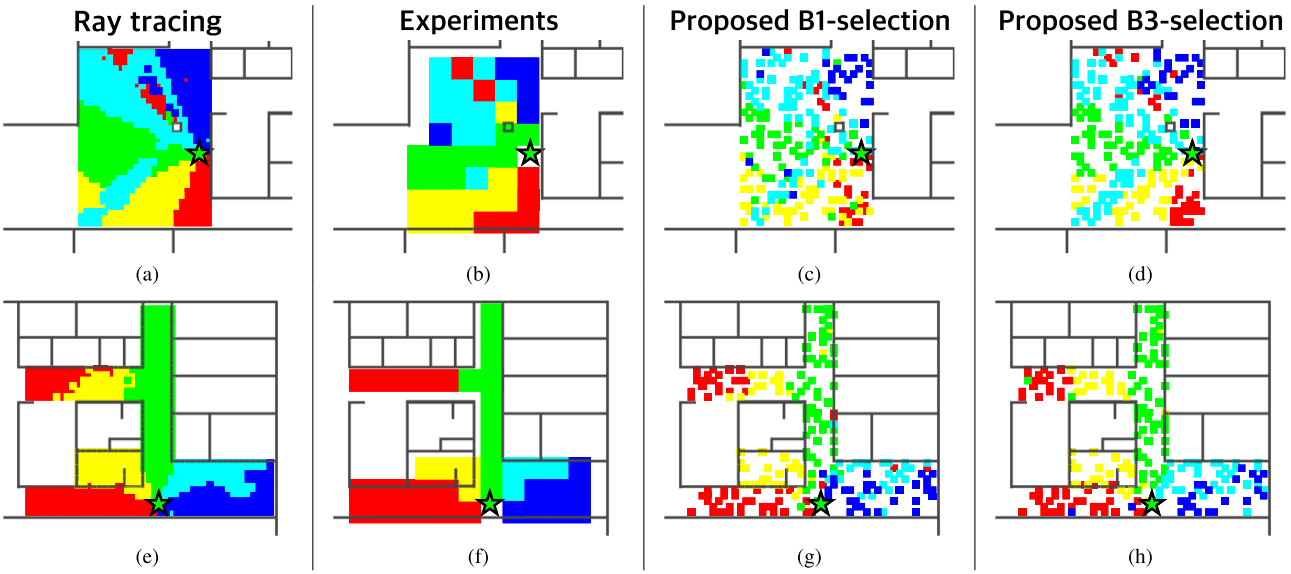

FIGURE 10. The results of beam-selection maps with different beam selection methods in lounge ((a), (b), (c), and (d)) and corridor ((e), (f), (g), and (h)) scenarios. Figs. (a) and (e) show the exhaustive search with the ray-tracing data. Figs. (b) and (f) show the exhaustive search with over-the-air measured data. Figs. (c) and (g) show the proposed B1-selection and Figs. (d) and (h) show the proposed B3-selection with the ray-tracing data.

a grid spacing of 2 m. Fig. 9(c) shows the transmitter and receiver setup, where the transmit horn antenna is placed on a pole, and the receiver lens antenna is placed on a moving desk.

Showing in Fig. 10 are the results of beam-selection maps with different beam selection methods. We considered the exhaustive search with the ray-tracing data (Fig. 10(a) and (e)), the exhaustive search with over-the-air experiment (Fig. 10(b) and (f)), and the proposed B1-selection (Fig. 10(c) and (g)) and B3-selection (Fig. 10(d) and (h)) with the ray-tracing data. From the results, we found two promising points. First, we confirmed that the distributions of selected beams of ray tracing are well-matched with the experiment. This fact supports our discussion above of ray tracing. Second, we validated the proposed beam selection algorithm also performs well and demonstrated graphically. As the results and discussions of Section IV-B indicate, the maps in Fig. 10 show that the proposed B3-selection outperforms the B1-selection.

V. CONCLUDING REMARKS

In this paper, we proposed a deep learning-based beam selection method that enables the initial beam establishment in 5G NR and 6G mmWave systems. To reduce the overhead of an SS burst, our proposed method returns probable candidates of proper beams by exploiting PDPs of sub-6 GHz channels. Via sub-6 GHz links, the proposed method can take advantage of channel characteristics before mmWave links are established. We also investigated the channel modelings of both bands and the SRS-based PDP estimation technique for 5G NR. Our 3D ray-tracing-based simulation results, which reflect the real environments, confirmed that the proposed beam selection shows high beam selection accuracy with parameters of the 5G NR standard. In the over-the-air experiments, beams selected with ray tracing matched well with the experiment, supporting our discussion based on 3D ray tracing. Our future work will consider multi-cell coordination and designing multi-user beam selection. We will also conduct a comparative study of our proposed beam selection and other deep learning-based methods.

REFERENCES

[1] Y.-G. Lim, T. Jung, K. S. Kim, C.-B. Chae, and R. A. Valenzuela, "Waveform multiplexing for new radio: Numerology management and 3D evaluation," *IEEE Wireless Commun.*, vol. 25, no. 5, pp. 86–94, Oct. 2018.
[2] T. S. Rappaport, S. Sun, R. Mayzus, H. Zhao, Y. Azar, K. Wang, G. N. Wong, J. K. Schulz, M. Samimi, and F. Gutierrez, "Millimeter wave mobile communications for 5G cellular: It will work!" *IEEE Access*, vol. 1, pp. 335–349, 2013.
[3] W. Roh, J.-Y. Seol, J. Park, B. Lee, J. Lee, Y. Kim, J. Cho, K. Cheun, and F. Aryanfar, "Millimeter-wave beamforming as an enabling technology for 5G cellular communications: Theoretical feasibility and prototype results," *IEEE Commun. Mag.*, vol. 52, no. 2, pp. 106–113, Feb. 2014.
[4] M. Giordani, M. Polese, A. Roy, D. Castor, and M. Zorzi, "A tutorial on beam management for 3GPP NR at mmWave frequencies," *IEEE Commun. Surveys Tuts.*, vol. 21, no. 1, pp. 173–196, 1st Quart., 2019.
[5] M. Giordani, M. Polese, A. Roy, D. Castor, and M. Zorzi, "Standalone and non-standalone beam management for 3GPP NR at mmWaves," *IEEE Commun. Mag.*, vol. 57, no. 4, pp. 123–129, Apr. 2019.
[6] C. Jeong, J. Park, and H. Yu, "Random access in millimeter-wave beamforming cellular networks: Issues and approaches," *IEEE Commun. Mag.*, vol. 53, no. 1, pp. 180–185, Jan. 2015.
[7] C. N. Barati, S. A. Hosseini, S. Rangan, P. Liu, T. Korakis, S. S. Panwar, and T. S. Rappaport, "Directional cell discovery in millimeter wave cellular networks," *IEEE Trans. Wireless Commun.*, vol. 14, no. 12, pp. 6664–6678, Dec. 2015.
[8] J. Choi, "Beam selection in mm-wave multiuser MIMO systems using compressive sensing," *IEEE Trans. Commun.*, vol. 63, no. 8, pp. 2936–2947, Aug. 2015.
[9] J. C. Aviles and A. Kouki, "Position-aided mm-wave beam training under NLOS conditions," *IEEE Access*, vol. 4, pp. 8703–8714, 2016.

[10] S.-Y. Lien, Y.-C. Kuo, D.-J. Deng, H.-L. Tsai, A. Vinel, and A. Benslimane, "Latency-optimal mmWave radio access for V2X supporting next generation driving use cases," *IEEE Access*, vol. 7, pp. 6782–6795, 2019.

[11] C.-W. Weng, B. P. S. Sahoo, C.-C. Chou, and H.-Y. Wei, "Efficient beam sweeping paging in millimeter wave 5G networks," in *Proc. IEEE Int. Conf. Commun. Workshops (ICC Workshops)*, May 2018, pp. 1–6.

[12] J. Schmidhuber, "Deep learning in neural networks: An overview," *Neural Netw.*, vol. 61, pp. 85–117, Jan. 2015.

[13] T. O'Shea and J. Hoydis, "An introduction to deep learning for the physical layer," *IEEE Trans. Cognit. Commun. Netw.*, vol. 3, no. 4, pp. 563–575, Dec. 2017.

[14] N. Samuel, T. Diskin, and A. Wiesel, "Deep MIMO detection," in *Proc. IEEE 18th Int. Workshop Signal Process. Adv. Wireless Commun. (SPAWC)*, Jul. 2017, pp. 1–5.

[15] H. Ye, G. Y. Li, and B.-H. Juang, "Power of deep learning for channel estimation and signal detection in OFDM systems," *IEEE Wireless Commun. Lett.*, vol. 7, no. 1, pp. 114–117, Feb. 2018.

[16] X. Wei, C. Hu, and L. Dai, "Knowledge-aided deep learning for beamspace channel estimation in millimeter-wave massive MIMO systems," 2019, *arXiv:1910.12455*. [Online]. Available: http://arxiv.org/abs/1910.12455

[17] H. Huang, S. Guo, G. Gui, Z. Yang, J. Zhang, H. Sari, and F. Adachi, "Deep learning for physical-layer 5G wireless techniques: Opportunities, challenges and solutions," *IEEE Wireless Commun.*, vol. 27, no. 1, pp. 214–222, Feb. 2020, doi: 10.1109/MWC.2019.1900027.

[18] J. Gante, G. Falciao, and L. Sousa, "Data-aided fast beamforming selection for 5G," in *Proc. IEEE Int. Conf. Acoust., Speech Signal Process. (ICASSP)*, Apr. 2018, pp. 1183–1187.

[19] V. Va, J. Choi, T. Shimizu, G. Bansal, and R. W. Heath, Jr., "Inverse multipath fingerprinting for millimeter wave V2I beam alignment," *IEEE Trans. Veh. Technol.*, vol. 67, no. 5, pp. 4042–4058, May 2018.

[20] V. Va, T. Shimizu, G. Bansal, and R. W. Heath, "Online learning for position-aided millimeter wave beam training," *IEEE Access*, vol. 7, pp. 30507–30526, 2019.

[21] A. Klautau, N. González-Prelcic, and R. W. Heath, "LIDAR data for deep learning-based mmWave beam-selection," *IEEE Wireless Commun. Lett.*, vol. 8, no. 3, pp. 909–912, Jun. 2019.

[22] A. Alkhateeb, S. Alex, P. Varkey, Y. Li, Q. Qu, and D. Tujkovic, "Deep learning coordinated beamforming for highly-mobile millimeter wave systems," *IEEE Access*, vol. 6, pp. 37328–37348, 2018.

[23] C. Anton-Haro and X. Mestre, "Learning and data-driven beam selection for mmWave communications: An angle of arrival-based approach," *IEEE Access*, vol. 7, pp. 20404–20415, 2019.

[24] P. Zhou, X. Fang, X. Wang, Y. Long, R. He, and X. Han, "Deep learning-based beam management and interference coordination in dense mmWave networks," *IEEE Trans. Veh. Technol.*, vol. 68, no. 1, pp. 592–603, Jan. 2019.

[25] Y. Long, Z. Chen, J. Fang, and C. Tellambura, "Data-Driven-Based analog beam selection for hybrid beamforming under mm-wave channels," *IEEE J. Sel. Topics Signal Process.*, vol. 12, no. 2, pp. 340–352, May 2018.

[26] T. Nitsche, A. B. Flores, E. W. Knightly, and J. Widmer, "Steering with eyes closed: mm-wave beam steering without in-band measurement," in *Proc. IEEE Conf. Comput. Commun. (INFOCOM)*, Apr. 2015, pp. 2416–2424.

[27] M. Alrabeiah and A. Alkhateeb, "Deep learning for mmWave beam and blockage prediction using sub-6GHz channels," 2019, *arXiv:1910.02900*. [Online]. Available: http://arxiv.org/abs/1910.02900

[28] O. Semiari, W. Saad, M. Bennis, and M. Debbah, "Integrated millimeter wave and Sub-6 GHz wireless networks: A roadmap for joint mobile broadband and ultra-reliable low-latency communications," *IEEE Wireless Commun.*, vol. 26, no. 2, pp. 109–115, Apr. 2019.

[29] B. Coll-Perales, J. Gozalvez, and M. Gruteser, "Sub-6 GHz assisted MAC for millimeter wave vehicular communications," *IEEE Commun. Mag.*, vol. 57, no. 3, pp. 125–131, Mar. 2019.

[30] Y.-G. Lim, Y. J. Cho, M. S. Sim, Y. Kim, C.-B. Chae, and R. A. Valenzuela, "Map-based millimeter-wave channel models: An overview, hybrid modeling, data, and learning," *IEEE Wireless Commun. Mag.*, submitted for publication.

[31] *Study on Channel Model for Frequencies From 0.5 to 100 GHz*, document 3GPP TR 38.901, Oct. 2019.

[32] Y. S. Cho, J. Kim, W. Y. Yang, and C. G. Kang, *MIMO-OFDM Wireless Communications With MATLAB*. Hoboken, NJ, USA: Wiley, 2010.

[33] T. Shuang, T. Koivisto, H.-L. Määttänen, K. Pietikäinen, T. Roman, and M. Enescu, "Design and evaluation of LTE-advanced double codebook," in *Proc. IEEE 73rd Veh. Technol. Conf. (VTC Spring)*, May 2011, pp. 1–5.

[34] *NR; Physical Channels and Modulation (Release 15)*, document 3GPP TS 38.211, 2019.

[35] *NR; Physical Layer Procedures for Control (Release 15)*, document 3GPP TS 38.213, 2019.

[36] C. K. Anjinappa and I. Guvenc, "Angular and temporal correlation of V2X channels across sub-6 GHz and mmWave bands," in *Proc. IEEE Int. Conf. Commun. Workshops (ICC Workshops)*, May 2018, pp. 1–6.

[37] S. M. Kay, *Fundamentals of Statistical Signal Processing*. Upper Saddle River, NJ, USA: Prentice-Hall, 1993.

[38] R. Schmidt, "Multiple emitter location and signal parameter estimation," *IEEE Trans. Antennas Propag.*, vol. AP-34, no. 3, pp. 276–280, Mar. 1986.

[39] Y.-J. Kim and G.-H. Im, "Pilot-symbol assisted power delay profile estimation for MIMO-OFDM systems," *IEEE Commun. Lett.*, vol. 16, no. 1, pp. 68–71, Jan. 2012.

[40] V. Erceg, S. J. Fortune, J. Ling, A. J. Rustako, and R. A. Valenzuela, "Comparisons of a computer-based propagation prediction tool with experimental data collected in urban microcellular environments," *IEEE J. Sel. Areas Commun.*, vol. 15, no. 4, pp. 677–684, May 1997.

[41] T. Kwon, Y.-G. Lim, B.-W. Min, and C.-B. Chae, "RF lens-embedded massive MIMO systems: Fabrication issues and codebook design," *IEEE Trans. Microw. Theory Techn.*, vol. 64, no. 7, pp. 2256–2271, Jul. 2016.

[42] Y. J. Cho, G.-Y. Suk, B. Kim, D. K. Kim, and C.-B. Chae, "RF lens-embedded antenna array for mmWave MIMO: Design and performance," *IEEE Commun. Mag.*, vol. 56, no. 7, pp. 42–48, Jul. 2018.

MIN SOO SIM (Student Member, IEEE) received the B.S. degree from the School of Integrated Technology, Yonsei University, in 2014, where he is currently pursuing the Ph.D. degree. His research interest includes emerging technologies for 5G/6G communications such as full-duplex radios and machine learning.

YEON-GEUN LIM (Member, IEEE) received the B.S. degree in information and communications engineering from Sungkyunkwan University, South Korea, in 2012, and the Ph.D. degree in engineering from Yonsei University, South Korea, in 2019, under the supervision of Prof. C.-B. Chae. He is currently a Staff Engineer with Samsung Electronics and has worked on 5G NR standardization in 3GPP RAN1. He was a Recipient/Corecipient of the Samsung Humantech Paper Award, from 2018 to 2019. He was involved in several industrial and national projects sponsored by Samsung Electronics, IITP, and KCA. He has published, in various research areas, 14 papers in international journals and conferences. His research interests include massive MIMO, new waveform, mm-Wave, full-duplex, system level simulation, and AI algorithms for physical layer wireless communications.

SANG HYUN PARK (Student Member, IEEE) received the B.S. degree in electronics engineering from Kwangwoon University, South Korea, in 2017. He is currently pursuing the Ph.D. degree with the School of Integrated Technology, Yonsei University, South Korea. His research interest includes emerging technologies for 5G/6G communications.

LINGLONG DAI (Senior Member, IEEE) received the B.S. degree from Zhejiang University, Hangzhou, China, in 2003, the M.S. degree (Hons.) from the China Academy of Telecommunications Technology, Beijing, China, in 2006, and the Ph.D. degree (Hons.) from Tsinghua University, Beijing, in 2011. From 2011 to 2013, he was a Postdoctoral Research Fellow of the Department of Electronic Engineering, Tsinghua University, where he was an Assistant Professor, from 2013 to 2016, and has been an Associate Professor, since 2016. His current research interests include massive MIMO, millimeter-wave communications, THz communications, NOMA, reconfigurable intelligent surface (RIS), and machine learning for wireless communications. He has coauthored the book *MmWave Massive MIMO: A Paradigm for 5G* (Academic Press, 2016). He has authored or coauthored more than 60 IEEE journal articles and more than 40 IEEE conference papers. He also holds 16 granted patents. He has received five IEEE best paper awards at the IEEE ICC 2013, the IEEE ICC 2014, the IEEE ICC 2017, the IEEE VTC 2017-Fall, and the IEEE ICC 2018. He has also received the Tsinghua University Outstanding Ph.D. Graduate Award, in 2011, the Beijing Excellent Doctoral Dissertation Award, in 2012, the China National Excellent Doctoral Dissertation Nomination Award, in 2013, the URSI Young Scientist Award, in 2014, the IEEE TRANSACTIONS ON BROADCASTING Best Paper Award, in 2015, the *Electronics Letters* Best Paper Award, in 2016, the National Natural Science Foundation of China for Outstanding Young Scholars, in 2017, the IEEE ComSoc Asia–Pacific Outstanding Young Researcher Award, in 2017, the IEEE ComSoc Asia–Pacific Outstanding Paper Award, in 2018, and the *China Communications* Best Paper Award, in 2019. He is an Area Editor of the IEEE COMMUNICATIONS LETTERS and an Editor of the IEEE TRANSACTIONS ON COMMUNICATIONS and the IEEE TRANSACTIONS ON VEHICULAR TECHNOLOGY. Particularly, he is dedicated to reproducible research and has made a large amount of simulation code publicly available.

CHAN-BYOUNG CHAE (Senior Member, IEEE) received the Ph.D. degree in electrical and computer engineering from The University of Texas at Austin, in 2008.

He is an Underwood Distinguished Professor with the School of Integrated Technology, Yonsei University, South Korea. Before joining Yonsei University, he was with Bell Labs, Alcatel–Lucent, Murray Hill, NJ, USA, from 2009 to 2011, as a Member of Technical Staff, and Harvard University, Cambridge, MA, USA, from 2008 to 2009, as a Postdoctoral Research Fellow. Prior to joining UT, he was a Research Engineer with the Telecommunications Research and Development Center, Samsung Electronics, Suwon, South Korea, from 2001 to 2005.

Dr. Chae is currently an IEEE ComSoc Distinguished Lecturer. He was the Recipient/Corecipient of the IEEE VTS Dan. E. Noble Fellowship Award, in 2008, the IEEE ComSoc AP Outstanding Young Researcher Award, in 2012, the IEIE/IEEE Joint Award for Young IT Engineer of the Year, in 2014, the KICS Haedong Young Scholar Award, in 2013, the *IEEE Signal Processing Magazine* Best Paper Award, in 2013, the Yonam Research Award from LG Yonam Foundation, in 2016, the IEEE INFOCOM Best Demo Award, in 2015, the Award of Excellence in Leadership of 100 Leading Core Technologies for Korea 2025 from the NAEK, in 2017, the IEEE DySPAN Best Demo Award, in 2018, the Young Engineer Award from the National Academy of Engineering of Korea (NAEK), in 2019, and the IEEE/KICS JOURNAL OF COMMUNICATIONS AND NETWORKS Best Paper Award, in 2018. He has served as an Editor for the IEEE TRANSACTIONS ON WIRELESS COMMUNICATIONS, from 2012 to 2017, and the IEEE TRANSACTIONS ON MOLECULAR, BIOLOGICAL, AND MULTI-SCALE COMMUNICATIONS, from 2015 to 2018. He is currently an Editor-in-Chief of the IEEE TRANSACTIONS ON MOLECULAR, BIOLOGICAL, AND MULTI-SCALE COMMUNICATIONS and a Senior Editor of the IEEE WIRELESS COMMUNICATIONS LETTERS. He has been served/serving as an Editor for the *IEEE Communications Magazine* and the IEEE WIRELESS COMMUNICATIONS LETTERS, since 2016.